

Superparticle Signatures: from PAMELA to the LHC

Daniel Feldman

Michigan Center for Theoretical Physics,
University of Michigan, Ann Arbor

Signatures of soft supersymmetry breaking at the CERN LHC and in dark matter experiments are discussed with focus drawn to light superparticles, and in particular light gauginos and their discovery prospects. Connected to the above is the recent PAMELA positron anomaly and its implications for signatures of SUSY in early runs at the Large Hadron Collider. Other new possibilities for physics beyond the Standard Model are also briefly discussed.

1. Dual Probes of SUSY

We review here testable predictions of high scale models with universal and non universal soft [supersymmetry]¹ breaking within the framework of applied supergravity (SUGRA) and effective models of string theories with D-branes supporting chiral gauge theories (for recent related reviews see [2,3]). Common to all these models are the ingredients needed for working in the predictive SUGRA framework, namely: (a) an effective Kähler metric which generally depends on moduli, (b) a gauge kinetic function also dependent on such scalars, and (c) a superpotential comprised of visible and hidden sector fields and a bilinear term for the Higgses.

An important set of predictions of the models discussed here is that they can offer the possibility of a relatively light gluino and electroweak gauginos with dark matter which is naturally Majorana. Thus the confluence of LHC signatures and signatures of dark matter play a central role in understanding the predictions of the above models. This connection is illuminated through knowledge of the possible sparticle mass hierarchies that can arise [4]. These mass hierarchies include the possibility of light scalars. However, naturalness/radiative electroweak symmetry breaking (REWSB) tend to point us to light gauginos and heavy squarks which generally occur on the upper Hyperbolic Branch (HB) of REWSB [6] often re-

ferred to as the focus point (FP) region. This region naturally arises in the minimal supergravity framework [7] and its extensions which are typically perturbations around universality.

Towards the end of this overview we will further discuss the connection between dark matter and the LHC, but more specifically in terms of the link between the WMAP data and the recent PAMELA positron excess [8]. Should the PAMELA anomaly be attributed to SUSY dark matter, the eigen-composition of the LSP plays a very relevant role. In addition, the composition of the LSP has important implications for collider signatures, and thus a direct bearing on the discovery prospects of SUSY at LHC, as well as the very nature of how dark matter was produced in the early universe.

2. Resolving the Sparticle Landscape

We begin with the Sparticle Landscape[4]. Of the 32 massive particles predicted in the MSSM, the number of ways in which the sparticle masses can stack up in their mass hierarchy is a priori undetermined unless an underlying framework is specified. Thus, if the 32 masses are treated as essentially all independent, then aside from sum rules on the Higgs, sfermions, and gaugino masses, and without imposition of any phenomenological constraints, the number of hierarchical patterns for all 32 sparticles could be as many as $O(10^{25-28})$ or larger. One may compare this with the landscape of string vacua in type II strings which lead to $O(10^{1000})$ possibilities.

¹For recent clear reviews see [1]

However, the number of superparticle mass hierarchies is reduced enormously in predictive frameworks such as supergravity models with REWSB.

Upon carrying out a mapping of the parameter space of the minimal SUGRA framework for the first four particles (discounting the lightest Higgs whose mass is constrained over a ~ 25 GeV range) we find 22 possible mass patterns consistent with all known collider and cosmological constraints. We label these as mSUGRA pattern 1 (mSP1) through mSUGRA pattern 22 (mSP22), the first 16 arising for $\mu > 0$ and the remaining for $\mu < 0$ [4]. In Table(1) we exhibit these mass orderings. The groupings may be considered more simply in terms of the NLSP; thus there are Chargino Patterns (CPs) (mSP 1-4), Stau Patterns (SUPs) (mSP 5-10,17-19), Stop Patterns (SOPs) (mSP 11-13,20,21), Higgs Patterns (HPs) (mSP 14-16), and an isolated Neutralino Pattern (mSP 22).

By extending the minimal framework to include larger landscapes in SUGRA models with non universalities (NUSUGRA) and in D-brane models we find new mass hierarchies. For the NUSUGRA cases, motivated by flavour changing neutral current constraints, considered are the following three possibilities for the soft parameters at the GUT scale: (i) the Higgs sector (NUH): $M_{H_u, H_d} = m_0(1 + \delta_{H(u,d)})$ (ii) the third generation squark sector (NU3): $M_{q3} = m_0(1 + \delta_{q3})$, $M_{u3,d3} = m_0(1 + \delta_{tbR})$, and (iii) the gaugino sector (NUG): $M_{1,2,3} = m_{1/2}\{1, (1 + \delta_2), (1 + \delta_3)\}$.

The landscape analysis reveals a collection of new mass hierarchies not discussed in the literature; even in the minimal model. Indeed most of the mSP patterns do not appear in previous works. All of the Snowmass mSUGRA points (labeled SPS) are only of types mSP(1,3,5,7). Regarding the Post-WMAP points, these are predominantly stau-coannihilation models, and one model which resides on the Hyperbolic Branch. The CMS benchmarks classified as (Low/High) Mass (LM)/(HM) [32] do a better job of representing mSP1 which is one of several dominant patterns, however, again the mapping only covers mSP(1,3,5,7) (see [4] for details). One such example of a missing class of mass hierarchies are the Higgs Patterns mSP(14-16) (HPs)[4] which occur for large $\tan\beta$ in mSUGRA (but occur

mSP	Mass Pattern	μ
mSP1	$\tilde{\chi}_1^0 < \tilde{\chi}_1^\pm < \tilde{\chi}_2^0 < \tilde{\chi}_3^0$	μ_\pm
mSP2	$\tilde{\chi}_1^0 < \tilde{\chi}_1^\pm < \tilde{\chi}_2^0 < A/H$	μ_\pm
mSP3	$\tilde{\chi}_1^0 < \tilde{\chi}_1^\pm < \tilde{\chi}_2^0 < \tilde{\tau}_1$	μ_\pm
mSP4	$\tilde{\chi}_1^0 < \tilde{\chi}_1^\pm < \tilde{\chi}_2^0 < \tilde{g}$	μ_\pm
mSP5	$\tilde{\chi}_1^0 < \tilde{\tau}_1 < \tilde{l}_R < \tilde{\nu}_\tau$	μ_\pm
mSP6	$\tilde{\chi}_1^0 < \tilde{\tau}_1 < \tilde{\chi}_1^\pm < \tilde{\chi}_2^0$	μ_\pm
mSP7	$\tilde{\chi}_1^0 < \tilde{\tau}_1 < \tilde{l}_R < \tilde{\chi}_1^\pm$	μ_\pm
mSP8	$\tilde{\chi}_1^0 < \tilde{\tau}_1 < A \sim H$	μ_\pm
mSP9	$\tilde{\chi}_1^0 < \tilde{\tau}_1 < \tilde{l}_R < A/H$	μ_\pm
mSP10	$\tilde{\chi}_1^0 < \tilde{\tau}_1 < \tilde{t}_1 < \tilde{l}_R$	μ_+
mSP11	$\tilde{\chi}_1^0 < \tilde{t}_1 < \tilde{\chi}_1^\pm < \tilde{\chi}_2^0$	μ_\pm
mSP12	$\tilde{\chi}_1^0 < \tilde{t}_1 < \tilde{\tau}_1 < \tilde{\chi}_1^\pm$	μ_\pm
mSP13	$\tilde{\chi}_1^0 < \tilde{t}_1 < \tilde{\tau}_1 < \tilde{l}_R$	μ_\pm
mSP14	$\tilde{\chi}_1^0 < A \sim H < H^\pm$	μ_+
mSP15	$\tilde{\chi}_1^0 < A \sim H < \tilde{\chi}_1^\pm$	μ_+
mSP16	$\tilde{\chi}_1^0 < A \sim H < \tilde{\tau}_1$	μ_+
mSP17	$\tilde{\chi}_1^0 < \tilde{\tau}_1 < \tilde{\chi}_2^0 < \tilde{\chi}_1^\pm$	μ_-
mSP18	$\tilde{\chi}_1^0 < \tilde{\tau}_1 < \tilde{l}_R < \tilde{t}_1$	μ_-
mSP19	$\tilde{\chi}_1^0 < \tilde{\tau}_1 < \tilde{t}_1 < \tilde{\chi}_1^\pm$	μ_-
mSP20	$\tilde{\chi}_1^0 < \tilde{t}_1 < \tilde{\chi}_2^0 < \tilde{\chi}_1^\pm$	μ_-
mSP21	$\tilde{\chi}_1^0 < \tilde{t}_1 < \tilde{\tau}_1 < \tilde{\chi}_2^0$	μ_-
mSP22	$\tilde{\chi}_1^0 < \tilde{\chi}_2^0 < \tilde{\chi}_1^\pm < \tilde{g}$	μ_-

Table 1

The Sparticle Landscape of Mass Hierarchies in mSUGRA. In patterns mSP14,15,16 the LSP $\tilde{\chi}_1^0$ and the Higgs bosons (A, H) can actually switch their order. (From Refs.(1,3) of [4].)

more generally at lower values in NUSUGRA) where the CP odd/heavier CP even Higgses are in fact the lightest particles beyond the LSP neutralino and in some cases they can be even lighter (we remind the reader that the Higgses are R-Parity even). The HPs typically occur in the bulk and will be discussed further in the next section. For the large m_0 region with lower values of $m_{1/2}$ the mass hierarchy is dominantly composed of mSP1 located in the HB/FP region where the LSP has a strong Higgsino component, while there is also a bino branch of mSP1 in which the the lightest chargino and next heavier neutralino are very close in mass, really effectively degenerate. One also observes several more CPs

NUSP	Mass Pattern	Model
NUSP1	$\tilde{\chi}_1^0 < \tilde{\chi}_1^\pm < \tilde{\chi}_2^0 < \tilde{t}_1$	NU3, NUG
NUSP2	$\tilde{\chi}_1^0 < \tilde{\chi}_1^\pm < A \sim H$	NU3
NUSP3	$\tilde{\chi}_1^0 < \tilde{\chi}_1^\pm < \tilde{\tau}_1 < \tilde{\chi}_2^0$	NUG
NUSP4	$\tilde{\chi}_1^0 < \tilde{\chi}_1^\pm < \tilde{\tau}_1 < \tilde{l}_R$	NUG
NUSP5	$\tilde{\chi}_1^0 < \tilde{\tau}_1 < \tilde{\nu}_\tau < \tilde{\tau}_2$	NU3
NUSP6	$\tilde{\chi}_1^0 < \tilde{\tau}_1 < \tilde{\nu}_\tau < \tilde{\chi}_1^\pm$	NU3
NUSP7	$\tilde{\chi}_1^0 < \tilde{\tau}_1 < \tilde{t}_1 < A/H$	NUG
NUSP8	$\tilde{\chi}_1^0 < \tilde{\tau}_1 < \tilde{l}_R < \tilde{\nu}_\mu$	NUG
NUSP9	$\tilde{\chi}_1^0 < \tilde{\tau}_1 < \tilde{\chi}_1^\pm < \tilde{l}_R$	NUG
NUSP10	$\tilde{\chi}_1^0 < \tilde{t}_1 < \tilde{g} < \tilde{\chi}_1^\pm$	NUG
NUSP11	$\tilde{\chi}_1^0 < \tilde{t}_1 < A \sim H$	NUG
NUSP12	$\tilde{\chi}_1^0 < A \sim H < \tilde{g}$	NUG
NUSP13	$\tilde{\chi}_1^0 < \tilde{g} < \tilde{\chi}_1^\pm < \tilde{\chi}_2^0$	NUG
NUSP14	$\tilde{\chi}_1^0 < \tilde{g} < \tilde{t}_1 < \tilde{\chi}_1^\pm$	NUG
NUSP15	$\tilde{\chi}_1^0 < \tilde{g} < A \sim H$	NUG
DBSP1	$\tilde{\chi}_1^0 < \tilde{\tau}_1 < \tilde{\nu}_\tau < A/H$	DB
DBSP2	$\tilde{\chi}_1^0 < \tilde{\tau}_1 < \tilde{\nu}_\tau < \tilde{l}_R$	DB
DBSP3	$\tilde{\chi}_1^0 < \tilde{\tau}_1 < \tilde{\nu}_\tau < \tilde{\nu}_\mu$	DB
DBSP4	$\tilde{\chi}_1^0 < \tilde{t}_1 < \tilde{\tau}_1 < \tilde{\nu}_\tau$	DB
DBSP5	$\tilde{\chi}_1^0 < \tilde{\nu}_\tau < \tilde{\tau}_1 < \tilde{\nu}_\mu$	DB
DBSP6	$\tilde{\chi}_1^0 < \tilde{\nu}_\tau < \tilde{\tau}_1 < \tilde{\chi}_1^\pm$	DB

Table 2

New sparticle mass hierarchies above and beyond those in the minimal framework in NUSUGRA and the D-brane model. Here one has gluino NLSP (GNLSP) patterns as well as the possibility of a light sneutrino of the third generation as the NLSP. (From Refs.(2,3) of [4].)

where the NLSP is a chargino (mSP1-mSP4), and where mSP4 is rather special with a very light neutralino mass less than ~ 55 GeV. Bino dominated patterns include, for example, the (SUPs) mSP(5-10) and (SOPs) mSP(11-13). A large density of the model points also occur in the vicinity of a Higgs pole [10]. Many models generally arise also from coannihilations [9], for example, mSP(5,7) and mSP(11) arise respectively from $\tilde{\tau}_1 - \tilde{\chi}_1^0$ and $\tilde{t}_1 - \tilde{\chi}_1^0$ coannihilation [11], however many of the new patterns actually arise from a large mixture of thermal annihilations.

For the case of non universal SUGRA models, 15 new mass patterns are uncovered labeled

NUSP(1-15). In a class of models based on D-branes (to be discussed shortly), 6 more new patterns labeled as DBSP(1-6) are also revealed. A complete set of specific benchmarks for each pattern can be found in [4]. There are also patterns where the gluino is light and is the NLSP (\equiv GNLSP discussed in what follows) and where the sneutrino of the third generation is light and is the NLSP occurring in the NU and DB cases respectively as illustrated in Table(2).

3. Light Higgs Bosons and D-branes

Progress in D-brane model building (see e.g., [12,13,14,15,16,17,18,19,20,21,3]) has lead to testable predictions of related models which support chiral matter [22,23,4,24]. Here we discuss light Higgses and dark matter in the context of SUGRA and D-branes [4]. We first briefly summarize the model class studied in [17] which offers a concrete early example of an effective string model where the soft terms can be computed. The model employs toroidal orbifold compactifications based on $\mathcal{T}^6/\mathbb{Z}_2 \times \mathbb{Z}_2$ where \mathcal{T}^6 is taken to be a product of 3 \mathcal{T}^2 tori. This model has a moduli sector consisting of volume moduli t_m , shape moduli u_m ($m = 1, 2, 3$) and the axion-dilaton field s . Of special interest here is the Kähler metric of the m^{th} component of open strings which are split between common brane stacks $[a, a]$ and twisted open strings connecting different brane stacks $[a, b]$. The Kähler metric is deduced from dimensional reduction and T -duality generalizing the previous known result for the heterotic string [17]. The soft scalars are simple functions of the graviton mass, the stack angle, and moduli VEVs and are given in full in [17]. Specifically the parameter space consists of the gravitino mass $m_{3/2}$, the gaugino mass $m_{1/2}$, the tri-linear coupling A_0 (which is in general non-vanishing), $\tan \beta$, $\text{sign}(\mu)$, the stack angle α ($0 \leq \alpha \leq \frac{1}{2}$), and the F term VEVs through the Goldstino angle θ , and complex modular parameters Θ_{t_i} , Θ_{u_i} ($i = 1, 2, 3$). The latter parametrize the directionality of the Goldstino angles in the modular space and enter in the VEV of the F -term which are functions of the real part of the moduli.

From the analysis of the D-brane model it is found that the mass hierarchies are dominated

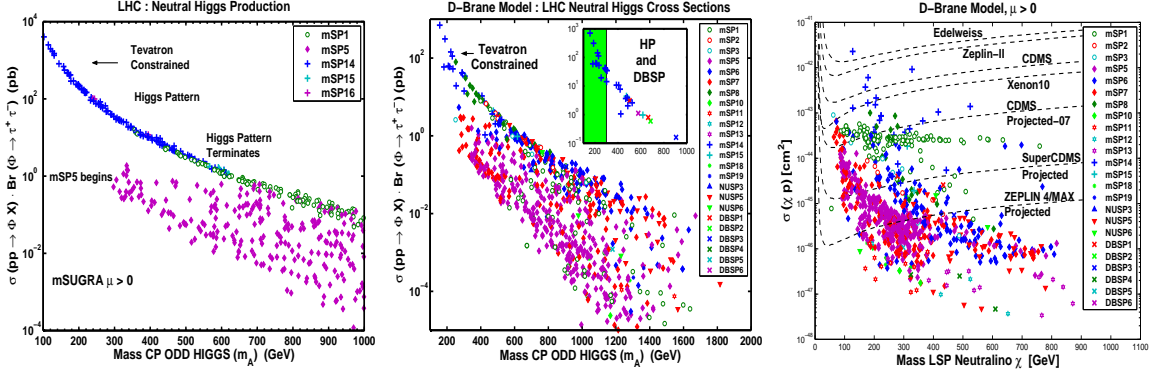


Figure 1. The neutral Higgs production cross section at the LHC in the 2τ mode as a function of the CP odd Higgs mass m_A for several patterns in mSUGRA (left panel) and (middle) all patterns arising in the D-brane model. The dark matter direct detection signature space for the D-brane model is also exhibited (right panel). (From Ref.(2) of [4].)

by the mSPs with only six new patterns (at isolated points) emerging. Of specific interest is that all the HPs (mSP14-mSP16) are seen to emerge in good abundance. Given in Fig.(1) (left panel) is the analysis of the neutral Higgs $[\Phi = h, H, A]$ production cross sections at the LHC in the 2τ mode for several patterns in the minimal SUGRA model with the dominant contributions to the cross section entering from gluon fusion and bottom quark annihilation processes. Similarly, in the middle panel of Fig.(1) are the Higgs production cross sections in the D-brane model, where all patterns seen in the D-brane model are exhibited. The analysis shows that the HPs dominate the Higgs production cross sections. One also finds that the $B_s \rightarrow \mu^+ \mu^-$ predictions constrain the HPs in this model[4]. The spin independent proton-LSP cross sections are given in the right panel of Fig.(1). Here also one finds that the Higgs Patterns typically give the largest scalar cross sections followed by the Chargino Patterns (mSP1-mSP3) and then by the Stau Patterns (which are dense in this model). Further, one finds a Wall of Chargino Patterns developing which enhances the discovery potential of these CPs (see also the middle panel of Fig.(2)). This Wall is consequence of the larger Higgsino

component of mSP1 which is also found in the DB model class [4].

4. Compressed Spectra in Intersecting D-brane Models

We consider next another class of D-brane models, motivated by the recent works of [16, 18, 19, 21]. The specific class of models we consider is with u moduli breaking. The model consists of a chiral particle spectrum arising from intersecting branes with supporting gauge groups $SU(3)_C \times SU(2)_L$ and $U(1)_a, U(1)_c, U(1)_d$ and $U(1)_Y$. Here, there is an anomalous $U(1) = U(1)_a + U(1)_d$ and the anomaly is cancelled via a Green-Schwarz mechanism (for an overview see [3]) giving a Stueckelberg mass to the $U(1)$ gauge boson (for recent reviews of the Stueckelberg mechanism see [25], [26]). The Kähler metric for the twisted moduli arising from strings stretching between stacks P and Q for the BPS 1/4 sector is taken in the form similar to [19], and more specifically of the form given in [22] where the gauge kinetic function is also deduced. The Kähler metric for BPS 1/2 brane configurations in this framework is given in [18]. In Table(3) a comparison is given of 2 model points, one from the D-brane model (labeled D6) and the other from mSUGRA, both of which sit in mSP3. We see from Table(3)

Sparticle type	D6 Mass/GeV	mSUGRA Mass/GeV
m_h	113.9	113.6
$\tilde{\chi}_1^0$	209.0	208.8
$\tilde{\chi}_1^\pm$	229.1	388.6
$\tilde{\chi}_2^0$	229.5	388.8
$\tilde{\tau}_1$	404.2	433.3
$\tilde{e}_R, \tilde{\mu}_R$	464.4	637.8
$\tilde{\tau}_1$	547.6	929.2
\tilde{g}	760.4	1181.4
$m_{\max=\tilde{s}, \tilde{d}_L}$	882.2	$m_{\max=\tilde{s}, \tilde{d}_L}$ 1210.4

D6 ($\tilde{B}, \tilde{W}, \tilde{H}_1, \tilde{H}_2$) (0.985, -.133, .104, -.0399) $\sigma_{\tilde{\chi}_1^0 p}^{\text{SI}} = 7.4 \times 10^{-9}$ pb $\Omega h^2 = 0.099$ co-annih.	mSUGRA ($\tilde{B}, \tilde{W}, \tilde{H}_1, \tilde{H}_2$) (0.994, -.017, .101, -.041) $\sigma_{\tilde{\chi}_1^0 p}^{\text{SI}} = 1.4 \times 10^{-8}$ pb $\Omega h^2 = 0.095$ $b\bar{b}, \tau\bar{\tau}$
---	---

Table 3

Illustration of the compressed spectra in the intersecting D-brane model (D6) and a comparison to a model in mSUGRA.

that these models have effectively the same LSP mass and light CP even Higgs mass. Observe also that there is a major violation of gaugino mass scaling in the D6 model relative to that of the mSUGRA model. Quite interestingly, the overall mass scale in the D6 model is much compressed relative to that of the mSUGRA model. This feature appears rather generic to the D6 models over the part of parameter space investigated. Thus while the LSP masses are effectively identical, the NLSP mass in the D6 model is about 160 GeV lighter than in the mSUGRA case considered. Further, the \tilde{g} is several hundred GeV lighter in the D6 case relative to the mSUGRA case and the heaviest sparticle in the D6 cases lies lower than the mSUGRA case by approximately 300 GeV. In Table(3) we see that the D6 LSP has a relatively larger wino component, while the LSP in the mSUGRA model is more of a mixed bino-Higgsino but with a stronger bino component. Both models give a relic density consistent with WMAP but do so in very different ways. The compressed mass scale has implications for

collider physics that requires further study.

5. Dark Matter and the LHC

We now turn to a very central idea; namely the correlation of LHC signals with dark matter direct detection signals. The correlation is exhibited in Fig.(2). The top panel gives an analysis at $L = 10 \text{ fb}^{-1}$ at $\sqrt{S} = 14 \text{ TeV}$ admitting only model points in the parameter space that generate at least 500 total SUSY events, for statistical significance, in the normalized channels $[2b\text{jets} + \text{jets} \geq 2]/N_{\text{SUSY}}$ vs $[1b\text{jet} + \text{jets} \geq 2]/N_{\text{SUSY}}$ and average P_T^{miss} vs $[0b\text{jets} + \text{jets} \geq 2]/N_{\text{SUSY}}$. The middle panels are 4 mSPs shown for illustration (for the full set see the 2nd Ref. of [4]) in the $\sigma_{\tilde{\chi}_1^0 p}^{\text{SI}}$ vs LSP signature space. Finally the bottom two panels show the effective mass distributions of sample benchmarks for different mSPs. A large separation among many of the hierarchical patterns can be seen in Fig.(2).

Indeed the mass hierarchies act as prism separating the landscape of signatures. The top left panel exhibits separation of CPs and HPs from SOPs and SUPs, with CPs and HPs occupying one region, and SOPs and SUPs occupy another in this signature space except for a very small overlap. This can be recast as ‘‘Higgsinos to one side, and binos the to other’’. The average missing P_T for each model point vs the fraction of events with $0b$ also shows a separation of the CPs and HPs from SOPs and SUPs. Further, mSP4 appears isolated residing in its own space. Even further, the middle panels exhibits the spin independent cross sections along with direct detection limits and indeed a remarkable separation of the mass patterns is achieved.

The left bottom panel shows distributions in effective mass where only trigger level cuts are imposed, while the right panel has post trigger level cuts imposed and they have been imposed globally for all the models considered (see the 3rd Ref. of [4] for these cuts). For the case when only trigger level cuts are imposed, the SOPs and CPs are highly peaked at lower values of effective mass, while the HPs and SUPs are much broader at higher effective mass. As is apparent, the trigger level cuts can have an enormous effect on the observability of these signals. Thus, imposing the

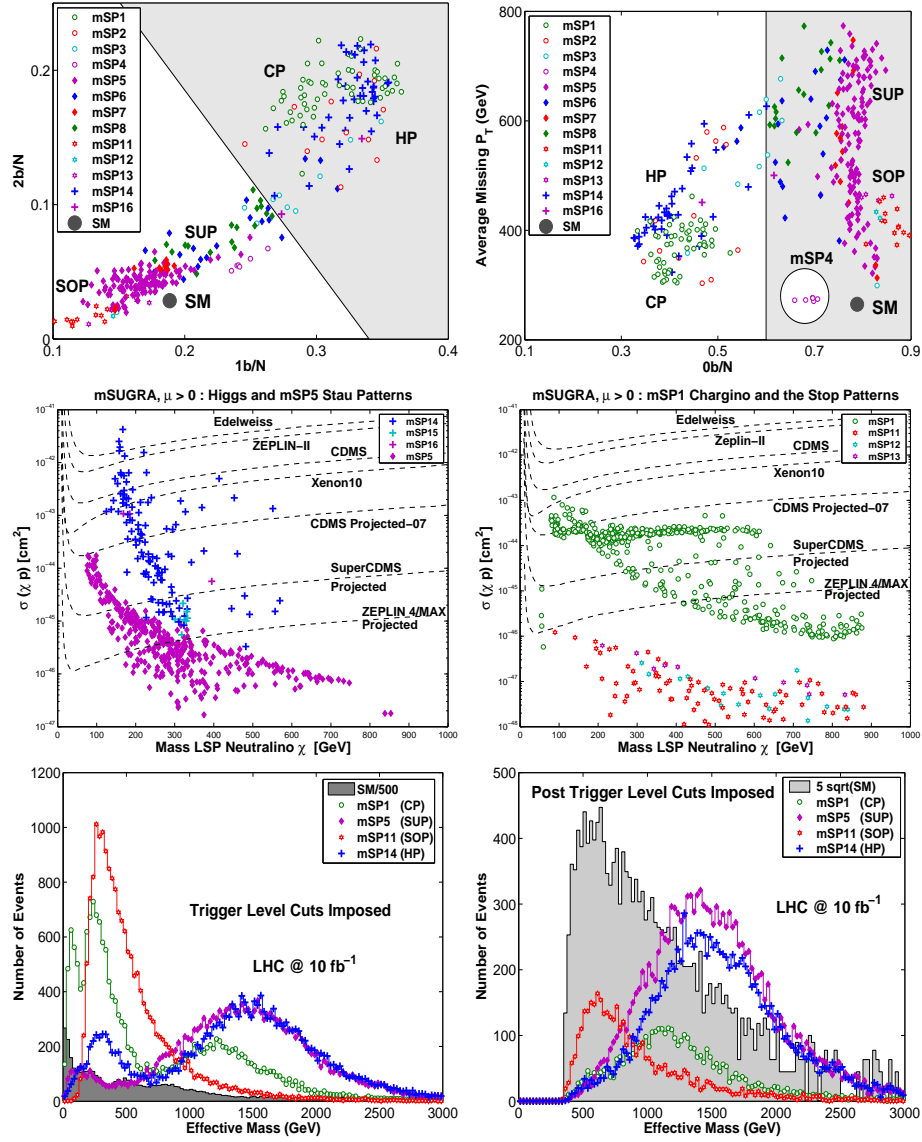


Figure 2. The top panel is full simulation of ~ 900 model points for minimal SUGRA at the LHC with 10/fb keeping only statistically significant model points. The middle panel has a larger set of data, but corresponds otherwise to same set of models in the top panel where the low mass points make the cut in the top panel. The bottom panels are the effective mass distribution for 4 benchmarks with the same cuts at the trigger and post trigger levels. One observes that the mass hierarchies act as a prism separating out various hierarchies into imprints on the dual signature spaces. Similar correlations for the non universal cases can be found in Refs.(2,3) of [4].

trigger level cuts globally on all classes of hierarchical mass patterns may disguise the signal. Additionally, the imposed post trigger level cuts kills the SOP and CP signals, while the SUPs and HPs signals remain relatively strong. Likewise, the missing P_T distributions for the SOPs and CPs are generally much narrower, while the HPs and SUPs are generally much broader. We observe these effects more generally in the minimal SUGRA model. The discovery prospects of SUSY will be directly tested by CMS and ATLAS [32] (see also [33]) and prospects continue to be explored at the Tevatron (for a sample of recent works by D0 & CDF see [34]). Triggering for different scenarios is quite important, in particular, as we illustrated here, the triggers need to be specialized for different mass hierarchies. There appears to be some attention now drawn this way for strategies in general [35].

6. LHC as a Gluino Factory, GNLSP, and Isomorphic GUT Models

The possibility of detecting the presence of a gluino close in mass to the LSP has been raised in [4] and recently has been studied in [31] and in [29]. This situation arises in supergravity models with non universalities in the gaugino mass sector [4] and can more specifically come about when the GUT symmetry is broken by a F term in $SU(5)$, $SO(10)$, and E_6 models. In the analysis of [29] it is found that a gluino NLSP (GNLSP) arises from such GUT models in the presence of an additional singlet. Thus what is minimally necessary for a GNLSP in these GUT models is a combination of GUT symmetry breaking in the gaugino mass term sector with two irreducible representations; a linear combination of a singlet and a non-singlet F term. In this case an interesting phenomenon arises in that models with the same $r \equiv (M_2 - M_1)/(M_3 - M_1)$ can be made isomorphic under redefinitions and scalings in the gaugino sector. Therefore, in essence, models with the same value of r would in fact be equivalent, or phenomenologically indistinguishable, when taken in a linear combination of breakings including singlets.

One finds that there are several possibilities for which the GNLSP class of models can arise that

fall under the isomorphic class of gaugino mass models. Considered more generally are 3 classes of models. (A) GNLSP_A: Here r takes the common value over several models: $(M_1 : M_2 : M_3) = (-1/2 : -3/2 : 1)$, $(19/10 : 5/2 : 1)$, $(-1/5 : -1 : 1)$; all of which map into $r = -2/3$. (B) GNLSP_B: This is a model specific to E_6 with F type breaking with **2430** plet such that [30] $E_6 \rightarrow SU(6)'' \times SU(2)_L (2430 \rightarrow (189, 1))$ which gives $M_1 : M_2 : M_3 = 0 : 0 : 1$. This model can generate a gluino as the NLSP upon the addition of breaking with a singlet. (C) GNLSP_C: Here r is free and thus defining $r = \delta_2/\delta_3$, the gaugino masses at the GUT scale may be parametrized as discussed earlier and can be varied independently. Model GNLSP_C contains models GNLSP_{A,B} as sub cases. For all the three models a GNLSP requires δ_3 to lie in the range $(-0.9, -0.8)$. We also note that from the analysis of [30] one can discern several other set of models which have a common value of r , i.e other models such as (A). Further examples of these isomorphisms are given in [29] along with generalized sum rules on the gaugino masses.

An interesting property of the GNLSP class of models is that the relic density (RD) is controlled by gluino coannihilations [27,28], and one has that $\langle \sigma_{\text{eff}} v \rangle$ to be integrated has a cross section well approximated by [29] $\sigma_{\text{eff}} \simeq \sigma_{\tilde{g}\tilde{g}} \gamma_{\tilde{\chi}_1^0}^2 \left(\gamma^2 + 2\gamma \frac{\sigma_{\tilde{\chi}_1^0 \tilde{g}}}{\sigma_{\tilde{g}\tilde{g}}} + \frac{\sigma_{\tilde{\chi}_1^0 \tilde{\chi}_1^0}}{\sigma_{\tilde{g}\tilde{g}}} \right)$, where $\gamma = \gamma_{\tilde{g}}/\gamma_{\tilde{\chi}_1^0}$ and where γ_i are defined in the standard notation of Ref. [9]. Thus for example, a typical set of annihilations *for a bino LSP* that contribute to the RD enter with weights $\tilde{\chi}_1^0 \tilde{\chi}_1^0 \rightarrow t\bar{t} (\lesssim 3\%)$, $\tilde{\chi}_1^0 \tilde{\chi}_1^0 \rightarrow \tau^+ \tau^- (\sim 1\%)$, $\tilde{\chi}_1^0 \tilde{g} \rightarrow t\bar{t} (\lesssim 3\%)$, $\tilde{g}\tilde{g} \rightarrow gg (\sim 50\%)$, $\tilde{g}\tilde{g} \rightarrow q\bar{q} (\sim 40\%)$. We also find cases where the GNLSP emerges without significant coannihilation which occurs when the LSP has a significant Higgsino component [29]. In either case there is a typical mass splitting of $\Delta_{\tilde{g}\tilde{\chi}_1^0} \equiv (m_{\tilde{g}} - m_{\tilde{\chi}_1^0})/m_{\tilde{\chi}_1^0} \in (0.08 - 0.20)$. Non-perturbative effects, namely a Sommerfeld Enhancement of $\langle \sigma_{\text{eff}} v \rangle$, i.e. reduction of $(\Omega h^2)_{\tilde{\chi}_1^0}$, requires $\Delta_{\tilde{g}\tilde{\chi}_1^0}$ increase by (2 to 3)% for $m_{\tilde{g}} \lesssim \text{TeV}$ to maintain $(\Omega h^2)_{\tilde{\chi}_1^0} \in \text{WMAP}$ [28,29]. We also find, that beyond the compression of the gluino mass in GNLSP models, there is a 2nd gener-

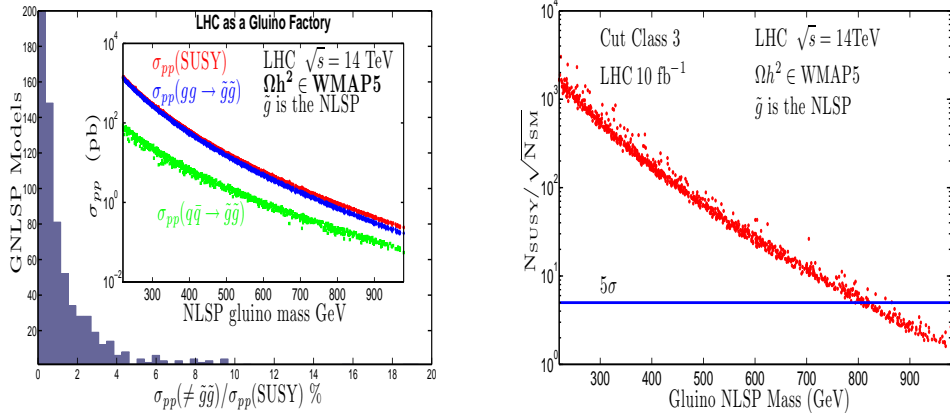


Figure 3. Gluino as the NLSP (GNLSP). Through \tilde{g} coannihilation WMAP relic density constraints are satisfied for \tilde{g} masses as light as a few hundred GeV and up to a TeV under naturalness assumptions. An overwhelming dominance of \tilde{g} production is observed [29].

ation slepton-squark degeneracy (SSD) and in some cases an inversion where these sleptons are heavier than the squarks [29].

The dominant SM backgrounds for GNLSP models at the LHC are from QCD, Z/W + jets, $b\bar{b}$, and $t\bar{t}$ and therefore one can cut on large $\Delta\phi(\text{jet}_1, \text{jet}_2)$ to suppress the QCD background due to light quark flavours and $b\bar{b}$ as well as $t\bar{t}$. We reject isolated e/μ from background W/Z leptonic decays and it is found that the e/μ veto significantly enhances the GNLSP signals over the SM background. Specific cuts are given in [29].

That the LHC will turn into a gluino factory if the GNLSP model is realized is seen in Fig.(3). Fig.(3) shows that a gluino NLSP consistent with the two sided WMAP relic density constraints can span the entire range from ~ 220 GeV to almost a TeV over the parameter space investigated. This analysis includes the radiative decay of the gluino, which can in some cases dominate the branching fractions of the gluino. As can be seen from Fig.(3), with just $10/\text{fb}$ a GNLSP can be discovered up to about 800 GeV and thus if the gluino and neutralino masses are split over a narrow gap, this mass hierarchy at the LHC can be tested into the TeV region [29].

7. Connecting PAMELA and the LHC

The connection between colliders and dark matter has become increasingly relevant due to new data released by the PAMELA collaboration indicating an excess in positron flux in the halo. In SUSY models ² with MSSM spectra annihilations of $\tilde{\chi}_1^0 \tilde{\chi}_1^0 \rightarrow WW, ZZ$ are dominant possible sources of positrons in the energy range of interest. The WW production can lead to a sufficiently large cross sections in the halo to account for the PAMELA anomaly (for recent related work see [36,37,38,39,40]). For a pure wino the halo cross section for the WW mode for $m_{\tilde{\chi}_1^0} \sim (180 - 200)$ GeV can be as large as $\sim 10^{-24} \text{cm}^3/\text{s}$, yet the mass splitting between $m_{\tilde{\chi}_1^\pm}$ and $m_{\tilde{\chi}_1^0}$ is squeezed to be order the pion mass when the spectrum is MSSM like. However, the PAMELA data can be fit when the LSP has a non-negligible Higgsino component, and in such a case, the mass gap between $m_{\tilde{\chi}_1^\pm}$ and $m_{\tilde{\chi}_1^0}$ opens up [40]. A mass splitting of order 10 GeV maintains a large enough wino component to produce a sufficiently large halo cross section, and leads to a significant change in the wave function of the LSP. This effect comes about from

²Discussed here are high scale models which lead to REWSB as in the previous sections.

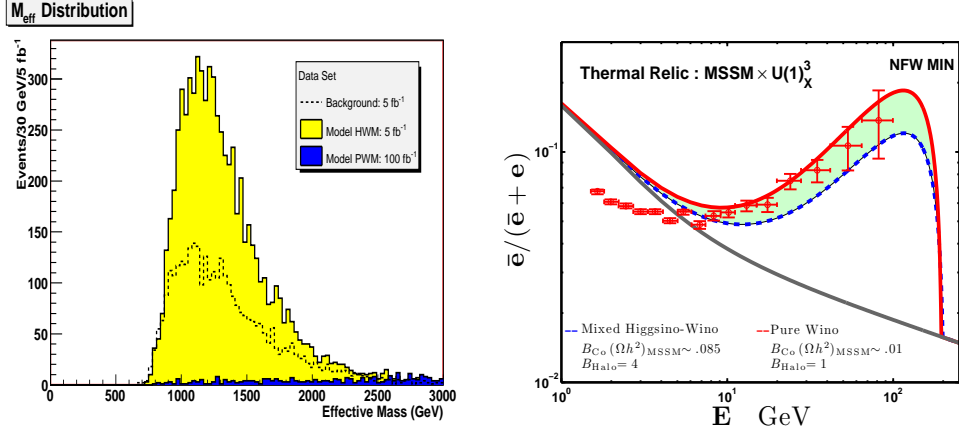


Figure 4. Left: Effective mass distribution for two models, a pure wino model (PWM) (blue/dark) which is on the floor even with $L = 100/\text{fb}$ in this model, and a mixed Higgsino-Wino model (HWM) (yellow/light) which produces a strong signal with $L = 5/\text{fb}$. For cuts see [40]. Right: Both models can fit the PAMELA positron data with small clump factors $\lesssim 5$, while the HWM can give rise to satisfaction of the WMAP data. Both models are capable of satisfying the \bar{p} constraint for a MIN diffusion model [40].

non universalities in gaugino masses, and can occur if there is, for example, a relatively large reduction of both the $SU(2)$ and $SU(3)$ gaugino masses at the GUT scale relative to the pure wino, where the pure wino can come about from a reduced $SU(2)$ gaugino mass. For this Higgsino-wino model (HWM) the LSP also has a relatively large bino component (we still call it HWM to distinguish it from the pure wino) and most importantly there is a compression of the colored sparticle masses opening up detectable signals at the LHC while the PAMELA data is also fit [40] (see Fig.(4) for one such comparison). The Higgsino content also leads to detectable spin independent cross section that can be observed with the CDMS and XENON-10 experiments [43]. The mass splitting also leads to a LSP which suffers less from the coannihilations with the chargino. The correct relic density prediction can be obtained from the presence of extra $U(1)_X$ gauge factors and thus the presence of extra Majorana matter arising from the hidden sector. The extra Majorana matter is naturally extra weakly interacting due to electroweak constraints. However it supplies extra degrees of freedom to the relic abundance of the LSP through coannihilations

and therefore *enhances* the relic density of the LSP neutralino. This is maximized for the HWM over the pure wino due to the lifting of the mass degeneracy for the HWM. This general concept of boosting the relic density of a thermal neutralino through coannihilations appeared earlier in [41] as well as in [42] in different contexts. If indeed the PAMELA data is due to neutralino annihilations in the halo, with the contributing annihilations controlled by MSSM interactions, the high energy $e^+ + e^-$ flux reported by FERMI must be dominantly a consequence of other astrophysical sources such as pulsars (see e.g. [46,37]).

On the other hand, dark matter annihilations which have a significant direct production of positrons through a pole [44] can simultaneously explain the PAMELA data as well as the WMAP data. For models which directly produce leptons, the high energy flux can be fit within the confines of the current experimental data (see [44] and [45]). For the case of a Breit-Wigner enhancement in the galactic halo [44] the fits to both the fluxes and WMAP data are made possible due to the spreading of $\langle\sigma v\rangle$ when integrating $\langle\sigma v\rangle$ up to the freeze out temperature in the vicinity of the pole. This may hint at a very narrow Z' which cou-

ples with hypercharge enhanced couplings to the SM fermions, and couples vectorially through a Stueckelberg field to a dark dirac fermion[47].

8. Conclusions

Low lying SUSY spectra, which sit in specific mass hierarchies, reveal that SUGRA and D-brane models have early discovery prospects at the LHC. These mass hierarchical patterns can be resolved by combining dark matter signatures and LHC signatures of new physics. Emphasized also was the possibility of a light chargino and a gluino that can surface with early runs at the LHC. Included in the discussion was the recently explored class of GUT models that yield a gluino as the NLSP (GNLSP) which satisfy WMAP constraints via gluino coannihilations and also give rise to signals at the LHC which are overwhelmingly dominated by gluino production. Several models reviewed have light SUSY Higgses and mass hierarchies involving these light Higgses are expected to be tested further in the next round of experiments.

Also discussed was the PAMELA positron excess which can be explained by SUSY dark matter in high scale models. Such a prediction depends importantly on the eigen decomposition of the LSP. A splitting of the chargino and LSP mass plays a central role in the observational prospects of these models. It is found that high scale models can predict a LSP with a non-negligible Higgsino component that can fit PAMELA and produce easily detectable LHC signatures, while a pure wino will be rather difficult to observe should the SUSY scale be order a few TeV. The \bar{p} constraints on these models can be satisfied for a MIN diffusion model. WMAP constraints can be accommodated in the presence of extra $U(1)_X$ factors which lead to extra Majorana degrees of freedom of spectator states with suppressed interactions that enhance the relic density of a mixed Higgsino-wino LSP via coannihilations. We also briefly mentioned earlier work which can fit both the low and high energy flux data, as well as the WMAP data, via the presence of a pole³.

³The Breit-Wigner enhancement with fits to the PAMELA data first appeared in Ref. 1 of [44] where WMAP data was also fit (see also the last 4 Refs. of [47] & [25]).

This comes about via a very narrow Z' resonance. A discovery of this type of Z' at the Tevatron and/or LHC in the dilepton channel may point us to a dark dirac fermion with mass that is slightly larger than $M_{Z'}/2$ and thus lend further support for this distinct possibility of leptonic annihilations in the halo [47,44].

Acknowledgements: This research received funding from NSF grant PHY-0757959 as well as from the Office of the Vice-Provost of Northeastern University, and support from the Michigan Center for Theoretical Physics (MCTP) and DOE grant DE-FG02-95ER40899.

REFERENCES

1. P. Nath, [arXiv:hep-ph/0307123] in “Beyond the desert 2003”, *Berlin, Springer, 2004.*, L. Ibanez and G. Ross, *Comptes Rendus Physique* **8**, 1013 (2007).
2. P. Nath and P. Fileviez Perez, *Phys. Rept.* **441**, 191 (2007); T. Ibrahim and P. Nath, *Rev. Mod. Phys.* **80**, 577 (2008).
3. R. Blumenhagen, B. Kors, D. Lust and S. Stieberger, *Phys. Rept.* **445**, 1 (2007).
4. D. Feldman, Z. Liu and P. Nath, *Phys. Rev. Lett.* **99**, 251802 (2007); *Phys. Lett. B* **662**, 190 (2008); *JHEP* **0804**, 054 (2008).
5. H. Baer, X. Tata, arXiv:0805.1905 [hep-ph]; R. L. Arnowitt, et. al *Phys. Rev. Lett.* **100**, 231802 (2008); B. Altunkaynak, M. Holmes and B. D. Nelson, *JHEP* **0810**, 013 (2008); D. Feldman, Z. Liu and P. Nath, *Phys. Rev. D* **78**, 083523 (2008); *AIP Conf. Proc.* **1078**, 116 (2009); N. Bhattacharyya, A. Datta and S. Poddar, *Phys. Rev. D* **78**, 075030 (2008); C. F. Berger, et. al, *JHEP* **0902**, 023 (2009); S. Bhattacharya, et. al, arXiv:0907.3428.
6. K. L. Chan, U. Chattopadhyay and P. Nath, *Phys. Rev. D* **58**, 096004 (1998); J. L. Feng, K. T. Matchev and T. Moroi, *Phys. Rev. Lett.* **84**, 2322 (2000).
7. A. H. Chamseddine, R. L. Arnowitt and P. Nath, *Phys. Rev. Lett.* **49**, 970 (1982).
8. [WMAP Collaboration], *Astrophys. J. Suppl.* **180**, 330 (2009); [PAMELA Collaboration], *Nature* **458**, 607 (2009).

9. K. Griest and D. Seckel, Phys. Rev. D **43**, 3191 (1991).
10. P. Nath and R. L. Arnowitt, Phys. Rev. Lett. **70**, 3696 (1993).
11. J. R. Ellis, T. Falk, K. A. Olive and M. Srednicki, Astropart. Phys. **13**, 181 (2000); J. R. Ellis, K. A. Olive and Y. Santos, Astropart. Phys. **18**, 395 (2003).
12. I. Antoniadis, E. Kiritsis and T. N. Tomaras, Phys. Lett. B **486**, 186 (2000).
13. L. E. Ibanez, F. Marchesano and R. Rabadan, JHEP **0111**, 002 (2001).
14. M. Cvetič, G. Shiu and A. M. Uranga, Nucl. Phys. B **615**, 3 (2001).
15. P. Nath and T. R. Taylor, Phys. Lett. B **548**, 77 (2002).
16. D. Cremades, L. E. Ibanez and F. Marchesano, JHEP **0307**, 038 (2003).
17. B. Kors and P. Nath, Nucl. Phys. B **681**, 77 (2004).
18. D. Lust, P. Mayr, R. Richter and S. Stieberger, Nucl. Phys. B **696**, 205 (2004); D. Lust, S. Reffert and S. Stieberger, Nucl. Phys. B **706** (2005) 3.
19. A. Font, L. Ibanez, JHEP **0503**, 040 (2005).
20. B. Kors and P. Nath, Nucl. Phys. B **711** (2005) 112.
21. M. Bertolini, M. Billo, A. Lerda, J. F. Morales and R. Russo, Nucl. Phys. B **743**, 1 (2006).
22. G. L. Kane, P. Kumar, J. D. Lykken and T. T. Wang, Phys. Rev. D **71**, 115017 (2005).
23. G. L. Kane, P. Kumar and J. Shao, J. Phys. G **34**, 1993 (2007).
24. C. Chen, T. Li, V. Mayes, D. Nanopoulos, Phys. Rev. D **77**, 125023 (2008); J. A. Maxin, V. E. Mayes and D. V. Nanopoulos, arXiv:0908.0915 [hep-ph].
25. D. Feldman, Z. Liu and P. Nath, AIP Conf. Proc. **939**, 50 (2007).
26. P. Langacker, arXiv:0801.1345 [hep-ph]; arXiv:0909.3260 [hep-ph].
27. S. Profumo and C. E. Yaguna, Phys. Rev. D **69**, 115009 (2004).
28. S. Profumo, Phys. Rev. D **72**, 103521 (2005).
29. D. Feldman, Z. Liu and P. Nath, Phys. Rev. D **80**, 015007 (2009).
30. S. P. Martin, Phys. Rev. D **79**, 095019 (2009).
31. J. Alwall, M. P. Le, M. Lisanti and J. G. Wacker, Phys. Lett. B **666**, 34 (2008).
32. [CMS Collaboration], J. Phys. G **34**, 995 (2007); [The ATLAS Collaboration], arXiv:0901.0512 [hep-ex].
33. S. Yamamoto [ATLAS Collaboration], arXiv:0710.3953 [hep-ex]; T. Yetkin and M. Spiropulu [CMS Collaboration], Acta Phys. Polon. B **38**, 661 (2007).
34. M. D'Onofrio, SUSY 09 Plenary Session.
35. O. Jinnouchi, SUSY 09 Plenary Session.
36. P. Grajek, G. Kane, D. Phalen, A. Pierce and S. Watson, Phys. Rev. D **79**, 043506 (2009).
37. G. Kane, R. Lu and S. Watson, arXiv:0906.4765 [astro-ph.HE].
38. D. Hooper, A. Stebbins and K. M. Zurek, Phys. Rev. D **79**, 103513 (2009).
39. J. Hisano, M. Kawasaki, K. Kohri, K. Nakayama, Phys. Rev. D **79**, 063514 (2009).
40. D. Feldman, Z. Liu, P. Nath and B. D. Nelson, arXiv:0907.5392 [hep-ph]; PRD in Press.
41. D. Feldman, B. Kors and P. Nath, Phys. Rev. D **75**, 023503 (2007) [arXiv:hep-ph/0610133]; P. Nath, arXiv:hep-ph/0610414.
42. S. Profumo and A. Provenza, JCAP **0612**, 019 (2006) [arXiv:hep-ph/0609290].
43. [XENON Collaboration], Phys. Rev. Lett. **100**, 021303 (2008); [CDMS Collaboration], Phys. Rev. Lett. **102**, 011301 (2009).
44. D. Feldman, Z. Liu and P. Nath, Phys. Rev. D **79**, 063509 (2009), [arXiv:0810.5762 [hep-ph]]; W. L. Guo and Y. L. Wu, Phys. Rev. D **79**, 055012 (2009); X. J. Bi, X. G. He and Q. Yuan, Phys. Lett. B **678**, 168 (2009); F. Y. Cyr-Racine, S. Profumo and K. Sigurdson, arXiv:0904.3933 [astro-ph.CO].
45. D. Grasso *et al.* [FERMI-LAT Collaboration], arXiv:0905.0636 [astro-ph.HE].
46. V. Barger, Y. Gao, W. Y. Keung, D. Marfatia and G. Shaughnessy, Phys. Lett. B **678**, 283 (2009).
47. B. Kors and P. Nath, Phys. Lett. B **586**, 366 (2004); JHEP **0412**, 005 (2004); JHEP **0507**, 069 (2005); D. Feldman, Z. Liu and P. Nath, Phys. Rev. Lett. **97**, 021801 (2006); JHEP **0611**, 007 (2006); Phys. Rev. D **75**, 115001 (2007); K. Cheung and T. C. Yuan, JHEP **0703**, 120 (2007); P. Nath, arXiv:0812.0958 [hep-ph]; Z. Liu, arXiv:0910.0061 [hep-ph].